Synthesis, Crystal Chemistry and Magnetism of the Metal-rich Borides $M_xRh_{7-x}B_3$ (M = Cr, Mn, Ni; x = 0.39 – 1) with Th_7Fe_3-type Structure

Patrick R. N. Misse, Richard Dronskowski, and Boniface P. T. Fokwa

Institute of Inorganic Chemistry, RWTH Aachen University, 52066 Aachen, Germany

Reprint requests to B. P. T. Fokwa. Email: boniface.fokwa@ac.rwth-aachen.de

Z. Naturforsch. **2011**, *66b,* 1241 – 1247; received October 21, 2011

Powder samples and single crystals of the boride phases $M_xRh_{7-x}B_3$ (M = Cr, Mn, Ni; $x \leq 1$) have been synthesized from the elements using an arc-melting furnace under purified argon atmosphere in a water-cooled copper crucible. The new phases were characterized from single-crystal and powder X-ray diffraction, as well as semi-quantitative EDX measurements. The obtained phases crystallize in the hexagonal Th_7Fe_3 structure type (space group $P6_3mc$, no. 186, Z = 2). In all cases (M = Cr, Mn, Ni), M is found to preferentially mix with rhodium at only one (6*c*) of the three available rhodium positions. Pauli paramagnetism was observed in $Cr_xRh_{7-x}B_3$ ($x < 1$), whereas both Pauli and temperature-dependent paramagnetisms were found in $NiRh_6B_3$.

Key words: Boron, Rhodium, Transition Metal Borides, Site Preference, Crystal Structure, Th_7Fe_3 Type, Paramagnetism

Introduction

In the last few years some ternary transition metal borides of the general formula $M_xT_{7-x}B_3$ (M = Cr, Mn, Fe, Co, Ni; T = Ru, Rh; $0 < x \leq 1.5$) have been synthetized and structurally described in the Th_7Fe_3 structure type [1 – 3]. These crystallographic studies have revealed two different size-dependent substitutions of an element T by an element M in the corresponding binary phase T_7B_3 en route to the above mentioned ternaries. In MRh_6B_3 (M = Fe, Co) for instance [2, 3], M was found to mix with rhodium at only one (6*c* site) of the three crystallographic rhodium sites present in Rh_7B_3. However, after increasing the amount of iron in $FeRh_6B_3$ to produce $Fe_{1.3}Rh_{5.7}B_3$, the additional iron atoms substitute rhodium not only in the expected 6*c* site but also in another one (2*b*), thereby leaving only one 6*c* site unaffected. For the ruthenium-rich phases, $M_xRu_{7-x}B_3$ (M = Cr, Mn, Fe, Co, Ni; T = Ru, Rh; $0 < x < 1$), two out of three ruthenium sites are found to accommodate the M elements, with the exception of the M = Mn case where only the first 6*c* site is affected by the manganese substitution.

The magnetic properties of some of these phases have also been investigated, and ferromagnetic ordering was observed experimentally for $FeRh_6B_3$ and $CoRh_6B_3$ below Curie temperatures of 240 and 150 K, respectively. These results were correctly reproduced by first-principles density functional theory (DFT) calculations which additionally revealed indirect magnetic coupling between the iron (or cobalt) atoms *via* rhodium atoms to be responsible for the magnetic ordering [2]. In $M_{0.5}Ru_{6.5}B_3$ (M = Cr, Mn, Co, Ni), however, paramagnetism was observed in all cases, and no hint of magnetic ordering down to 4 K was found [4].

Motivated by the magnetic ordering found for MRh_6B_3 (M = Fe, Co) phases [2], the synthesis and characterization of new rhodium-rich phases containing other magnetically active 3*d* transition metals (M = Cr, Mn, Ni) was the next logical step. Herein, we report on the synthesis, crystal chemistry and magnetic properties of the new $M_xRh_{7-x}B_3$ (M = Cr, Mn, Ni; $0 < x \leq 1$) phases.

Results and Discussion

Phase analysis

The single phase $NiRh_6B_3$

All the available peaks of the X-ray powder diffractogram of $NiRh_6B_3$ could be assigned to the Th_7Fe_3 structure type. Thus, the synthesized product is a single phase (see Fig. 1). Its single-phase nature and the presence of the two transition metals were also correctly reproduced by EDX analysis. The refined lattice parameters of $NiRh_6B_3$ are in the same range as those found for the MRh_6B_3 (M = Fe, Co) phases

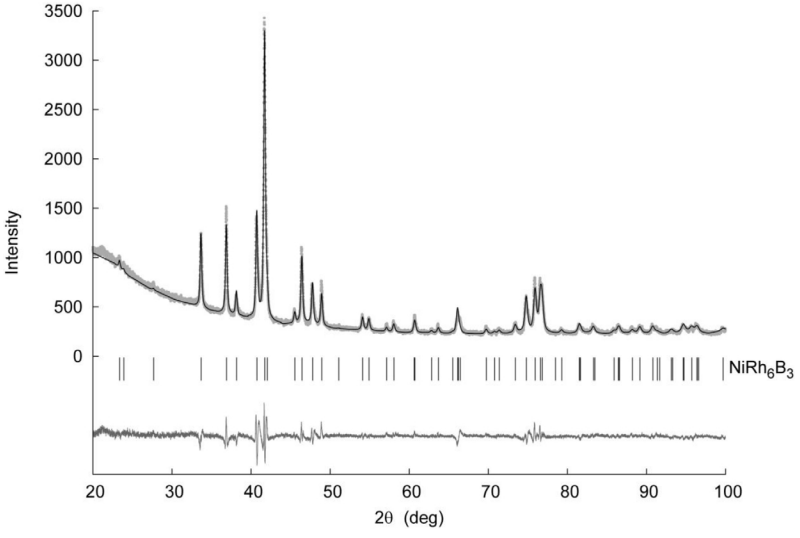

Fig. 1. Rietveld refinement of the powder X-ray data of the $NiRh_6B_3$ phase showing measured and fitted intensities (top), the position of the Bragg peaks (middle), and the difference intensity curve (bottom).

Table 1. Results of the Rietveld refinement for the ternary borides $M_xRh_{7-x}B_3$ (M = Cr, Mn, Ni).

Formula	$Cr_xRh_{7-x}B_3$	$Mn_xRh_{7-x}B_3$	$NiRh_6B_3$
Structure refinement	Rietveld, least-squares method		
Profile function	Pseudo-VOIGT		
Space group; Z	$P6_3mc$ (no. 186); 2		
Cell parameters			
a, Å	7.433(1)	7.461(1)	7.441(2)
c, Å	4.749(1)	4.766(1)	4.714(1)
V, Å^3	227.19(1)	229.77(1)	226.03(2)
R_{Bragg}	0.144	0.176	0.096
Main phase amount, %	~ 99	~ 97	100
Side phase [6]	$Rh_{0.75}Cr_{0.25}$	Rh	–

(see Table 1). However, they are all smaller than those reported for the binary phase Rh_7B_3 (a = 7.47, c = 4.78 Å, V = 230.9 Å^3) [5], as expected, because an element with a smaller atomic radius (M = Fe, Co or Ni) has substituted the larger rhodium atom in the parent Rh_7B_3 phase. The unit cell volume in the MRh_6B_3 (M = Fe, Co, Ni) series decreases with increasing atomic number of M (see Fig. 2). Although the decrease of the unit cell volume from $CoRh_6B_3$ to $NiRh_6B_3$ can be explained by a slight decrease of the atomic radius from Co to Ni, the same arguments become invalid for the Fe- and Co-cases for which an increase of the unit cell volume would have been expected. Therefore electronic and magnetic effects are also playing a great role (see below).

$Cr_xRh_{7-x}B_3$ and $Mn_xRh_{7-x}B_3$

For the starting compositions "$CrRh_6B_3$" and "$MnRh_6B_3$" a phase analysis of their X-ray powder

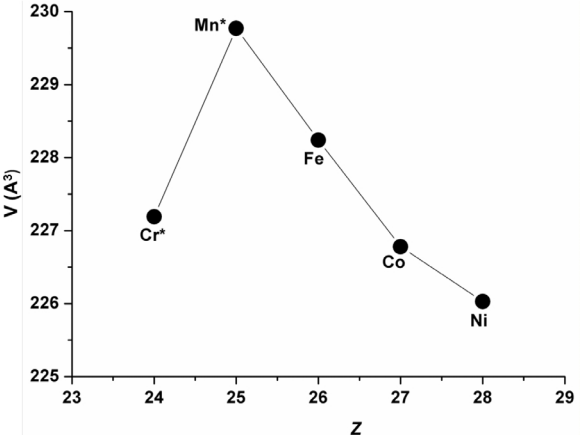

Fig. 2. Unit cell volume as a function of the atomic number Z (of M) for the MRh_6B_3 (M = Fe, Co, Ni) and $M_xRh_{7-x}B_3$ (M = Cr, Mn; $x < 1$) phases. *: presence of a minor side phase.

diffraction patterns revealed that the expected phase (Th_7Fe_3 structure type) was the main component of a two-phase product. Fig. 3 shows the Rietveld refinement of the powder X-ray pattern of the "$CrRh_6B_3$" product which contains a small amount of a side phase identified to be the intermetallic phase $Rh_{0.75}Cr_{0.25}$ [6], which is a Cr-doped elemental rhodium phase. Nevertheless, the refined lattice parameters of the main phase (see Table 1) fall in the same range as those obtained for the isotypic MRh_6B_3 (M = Fe, Co, Ni) single phases (see Fig. 2). Consequently, they are also smaller than those found for the binary Rh_7B_3, but unexpectedly larger than those of the Co-phase. The

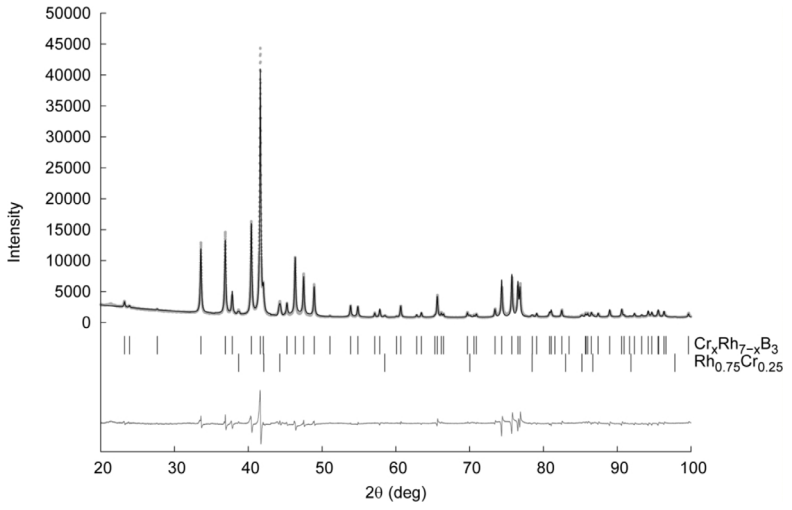

Fig. 3. Rietveld refinement of the powder X-ray data of $Cr_xRh_{7-x}B_3$ showing measured and fitted intensities (top), the position of the Bragg peaks of the two phases (middle), and the difference intensity curve (bottom).

Table 2. Crystallographic data and numbers pertinent to the single-crystal structure refinement of $Cr_{0.78(3)}Rh_{6.22(3)}B_3$ and $Mn_{0.39(3)}Rh_{6.61(3)}B_3$.

Formula	$Cr_{0.78(3)}Rh_{6.22(3)}B_3$	$Mn_{0.39(3)}Rh_{6.61(3)}B_3$
Formula weight, g mol^{-1}	713.60	733.61
Crystal size, mm^3	$0.08 \times 0.06 \times 0.04$	$0.08 \times 0.06 \times 0.04$
Crystal system	– hexagonal –	
Space group; Z	– $P6_3mc$ (no. 186); 2 –	
Cell parameters		
a, Å	7.4386(9)	7.4634(3)
c, Å	4.7541(9)	4.7644(2)
V, Å^3	227.81(6)	229.83(2)
Calcd. density, g cm^{-3}	10.40	10.60
Abs. coefficient μ, mm^{-1}	23.6	24.0
$F(000)$, e	628	644
θ-range, deg	$5.33 \leq 2\theta \leq 36.6$	$5.32 \leq 2\theta \leq 35.92$
hkl range	$-12 \leq h \leq 11$	$-11 \leq h \leq 12$
	$-11 \leq k \leq 12$	$-12 \leq k \leq 12$
	$-7 \leq l \leq 6$	$-7 \leq l \leq 7$
Reflections / R_{int}	3304 / 0.0277	3355 / 0.0227
Independent refls.	406	389
Obs. refls. $I \geq 2\sigma(I)$	404	386
Friedel pairs	176	155
No. of ref. parameters	22	21
GooF	1.22	1.25
R_1 / wR_2 (all data)	0.012 / 0.028	0.014 / 0.033
Diff. peak / hole, e Å^{-3}	0.82 / −0.89	0.88 / −0.91

formation of $Rh_{0.75}Cr_{0.25}$ indicates that the composition of the synthesized main phase may be different from the expected one ($CrRh_6B_3$). A single crystal analyzed by both single-crystal refinement (see crystal chemistry section) and EDX analysis yielded the chemical formula $Cr_{0.78(3)}Rh_{6.22(3)}B_3$, thereby confirming this assumption and also explaining why its volume is larger than that of the Co-based phase. In fact, the Cr-based phase is Rh-richer than the Co-based one and, therefore, must have a larger cell volume. Because the lattice parameters of the single crystal are nearly identical to those of the powder data (see Tables 1 and 2), the chemical formula of the Cr-based sample should be near that of the single crystal and may be generalized by $Cr_xRh_{7-x}B_3$ ($x \approx 0.78$).

The analysis of the powder pattern of "$MnRh_6B_3$" has revealed, beside the expected main phase (Th_7Fe_3 structure type), some unreacted elemental rhodium as a side phase. Nevertheless, the refined lattice parameters of the main phase (see Table 1) corroborate well those obtained for the aforementioned MRh_6B_3 (M = Fe, Co, Ni) and $Cr_xRh_{7-x}B_3$ ($x \approx 0.78$) phases. Although it is obvious that a ternary Mn-based phase has been synthesized, mainly because the lattice parameters of the synthesized sample differ significantly from those found for the binary Rh_7B_3, the same geometrical arguments used for the above-mentioned isotypic phases are not applicable in this case. In fact the lattice parameters of the Mn-based ternary phase are smaller than those of the binary Rh_7B_3, despite the fact that manganese has a larger atomic radius than rhodium. Consequently, and contrary to the other isotypic cases, electronic rather than geometric reasons are playing a key role in the rhodium substitution by manganese in the binary en route to the ternary phase. The presence of unreacted elemental rhodium as a side phase indicates, similar to the previous Cr case, that the expected stoichiometry was probably unachieved. Indeed the structure refinement of a single crystal as well as its subsequent EDX analysis have revealed the composition $Mn_{0.39(3)}Rh_{6.61(3)}B_3$. The manganese content

Atom	W. position	Occupancy	x	y	z	U_{eq} (Å^2)
$Cr_{0.78(3)}Rh_{6.22(3)}B_3$:						
Rh1	6*c*	1.0	0.87471(2)	$1-x$	0.32604(5)	0.00856(7)
*T*2	6*c*	Rh2:0.74(1) Cr2:0.26(1)	0.54442(2)	$1-x$	0.00067(8)	0.00926(9)
Rh3	2*b*	1.0	1/3	2/3	0.00381(11)	0.0079(1)
B	6*c*	1.0	0.1866(3)	$1-x$	0.2319(9)	0.0107(6)
$Mn_{0.39(3)}Rh_{6.61(3)}B_3$:						
Rh1	6*c*	1.0	0.87616(3)	$1-x$	0.32931(9)	0.00796(9)
*T*2	6*c*	Rh2:0.87(1) Mn2:0.13(1)	0.54404(3)	$1-x$	−0.00434(10)	0.00767(11)
Rh3	2*b*	1.0	1/3	2/3	0.00135(15)	0.00664(11)
B	6*c*	1.0	0.1872(4)	$1-x$	0.233(2)	0.0118(9)

Table 3. Atomic coordinates, and equivalent displacement parameters (U_{eq}) for $Cr_{0.78(3)}Rh_{6.22(3)}B_3$ and $Mn_{0.39(3)}Rh_{6.61(3)}B_3$. U_{eq} is defined as 1/3 of the trace of the orthogonalized U_{ij} tensors.

of this single crystal is, however, far lower than that of the loaded one. In fact, of all the elements used in this work, manganese has the lowest melting and boiling point [7], and therefore some manganese may have evaporated during the melting process ($T > 3000$ °C). We have also tried to verify this assumption by targeting another synthesis of the expected phase using manganese in excess (about 30 and 50 % more): Although the results indicate a slight increase of the lattice parameters as expected, the targeted phase was no longer the main phase (*ca.* 30 %) as a new phase with the probable formula "$Mn_{3-x}Rh_5B_{2+x}$" crystallizing with $Ti_3Co_5B_2$ structure type prevailed in both syntheses. An increase of the lattice parameters (*ca.* 1 Å^3 volume increment) was found, indicating an incorporation of more manganese in the new composition. Nearly the same volume increment (1.16 Å^3) was calculated for the volume obtained from the $Mn_{0.39(3)}Rh_{6.61(3)}B_3$ single crystal and that of the binary Rh_7B_3 phase, indicating that a significant change of the chemical formula is to be expected. Therefore, the maximum amount of manganese which may substitute rhodium in Rh_7B_3 cannot be obtained from these results, and single crystals are needed for this purpose. The targeted Mn-based compositions may therefore be generalized as solid solutions $Mn_xRh_{7-x}B_3$ ($x \geq 0.39$).

Crystal chemistry

The crystal structures of the three phases $NiRh_6B_3$, $Cr_{0.78(3)}Rh_{6.22(3)}B_3$ and $Mn_{0.39(3)}Rh_{6.61(3)}B_3$ were refined using the Rietveld method for the first and single-crystal methods for the second and third cases.

The single-phase nature of $NiRh_6B_3$ as well as EDX measurements of the metal ratio and the absence of single crystals implied that the use of the Rietveld method for structure refinement was unavoidable. For this purpose a structure model based on the single-crystal data of $FeRh_6B_3$ was used, but replacing iron by nickel. In this model, nickel is found with rhodium at only one of the three possible Wyckoff sites (two 6*c* sites and one 2*b*) occupied by rhodium in the binary Rh_7B_3. The straightforward refinement led to the results presented in Table 1. A statistical model was also tried, in which nickel was mixed with rhodium on all three possible Wyckoff sites, but the quality of the results was significantly worse than in the previous case. Therefore, the same size-dependent site preferential substitution found in the previously reported MRh_6B_3 (M = Fe, Co) is also observed in $NiRh_6B_3$.

For the Cr- and Mn-based phases, the single-crystal structure solutions and the subsequent refinements confirmed the previous model, the only difference being the low amount of chromium and manganese found in each phase. All relevant crystallographic data and experimental details of the data collections are listed in Table 2. The atomic coordinates and the displacement parameters are reported in Table 3, while Table 4 summarizes the selected interatomic distances. Excellent refinements were achieved in both cases; with final residual values $R_1 = 0.012$ and $wR_2 = 0.028$ for all 406 reflections and 22 parameters in the Cr-based phase, and $R_1 = 0.014$ and $wR_2 = 0.033$ for all 389 reflections and 21 parameters in the Mn-based case, with the final refined formulas $Cr_{0.78(3)}Rh_{6.22(3)}B_3$ and $Mn_{0.39(3)}Rh_{6.61(3)}B_3$. Although the two chemical formulas differ from those of the phases reported above, namely MRh_7B_3 (M = Fe, Co, Ni), all these Rh-based phases follow basically the same substitution path, and their compositions may be generalized by the formula $M_xRh_{7-x}B_3$ (M = Cr, Mn, Fe, Co, Ni with $0.39 \leq x \leq 1$).

A detailed description of the crystal structure has already been presented for $FeRh_6B_3$ [3] which is

Table 4. Selected interatomic distances (Å) in $Cr_{0.78(3)}Rh_{6.22(3)}B_3$ and $Mn_{0.39(3)}Rh_{6.61(3)}B_3$ ($T2$ = Rh2/Cr2 or Rh2/Mn2).

		$Cr_{0.78(3)}Rh_{6.22(3)}B_3$		$Mn_{0.39(3)}Rh_{6.61(3)}B_3$	
Rh1	-B	1×	2.086(5)	1×	2.090(6)
	-B[a]	2×	2.169(3)	2×	2.181(4)
	-Rh1	2×	2.796(1)	2×	2.773(1)
	-*T*2	2×	2.799(1)	2×	2.829(1)
	-Rh3	1×	2.811(1)	1×	2.829(1)
	-*T*2[a]	2×	2.825(1)	2×	2.843(1)
	-Rh1[a]	4×	2.873(1)	4×	2.870(1)
***T*2**	-B	2×	2.170(3)	2×	2.157(5)
	-*T*2	2×	2.638(1)	2×	2.640(1)
	-B[a]	2×	2.653(3)	2×	2.668(4)
	-Rh3	1×	2.720(1)	1×	2.724(1)
	-*T*2[a]	2×	2.729(1)	2×	2.746(1)
	-Rh1	2×	2.799(1)	2×	2.829(1)
	-Rh1[a]	2×	2.825(1)	2×	2.843(1)
	–Rh3[a]	1×	2.839(1)	1×	2.839(1)
	–Rh3[a]	1×	2.864(1)	1×	2.864(1)
Rh3	-B	3×	2.179(4)	3×	2.188(4)
	-*T*2	3×	2.720(1)	3×	2.724(1)
	-Rh1	3×	2.811(1)	3×	2.829(1)
	-*T*2[a]	3×	2.839(1)	3×	2.839(1)
	-*T*2[a]	3×	2.864(1)	3×	2.884(1)
B1	-Rh1	1×	2.086(5)	1×	2.090(6)
	-*T*2	2×	2.170(3)	2×	2.157(5)
	-Rh1[a]	2×	2.169(3)	2×	2.181(4)
	-Rh3	1×	2.179(3)	1×	2.188(4)

[a] Symmetry-related atom.

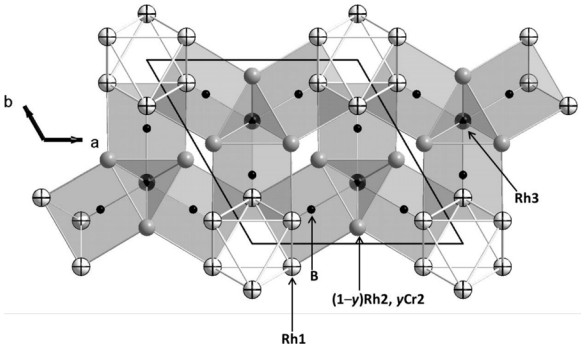

Fig. 4. Projection of the crystal structure of the ternary borides $M_xRh_{7-x}B_3$ (M = Cr, Mn, Fe, Co, Ni with $0.39 \leq x \leq 1$) along [001]. The octahedral $(Rh1)_6$ clusters and the boron-centered trigonal prisms are highlighted.

isostructural with the new phases. The two main characteristics of these structures are the boron-centered trigonal prisms built up by rhodium (Rh1, Rh3) and $T2$ (Rh2/M) atoms and the empty octahedral Rh_6 clusters (see Fig. 4). In general, the distances found in the Mn-based phase are larger than those found in the other cases, an expected behavior because of the larger lattice parameters measured for the former (see Fig. 2).

The interatomic distances found for $Cr_{0.78(3)}Rh_{6.22(3)}B_3$ in the single-crystal investigations are slightly smaller than those in $Mn_{0.39(3)}Rh_{6.61(3)}B_3$ (see Table 4). Likewise, they are slightly smaller than those observed in the binary compound Rh_7B_3. In both cases, ($Cr_{0.78(3)}Rh_{6.22(3)}B_3$ and $Mn_{0.39(3)}Rh_{6.61(3)}B_3$), the Rh–B and $T2$–B distances are the shortest ones in the structure with an average value of 2.17 Å, which is quite similar to that observed in $CoRh_6B_3$ (average 2.17 Å) [2], in $FeRh_6B_3$ (average 2.15 Å) [3] or in $Fe_{1.3}Rh_{5.7}B_3$ (average 2.13 Å) [1]. Even shorter interatomic distances between the boron and the rhodium atoms were found in the phases $ScRh_3B$ (2.04 Å) [8] and Ti_2Rh_6B (2.02 Å) [9], but in these perovskite-based phases boron is octahedrally coordinated. As observed in previous phases, these metal-boron bonding interactions are expected to be the strongest in these structures. Furthermore, in both Cr- and Mn-based phases the $T2$–$T2$ distances (average 2.68 Å) are shorter than the other distances to rhodium (Rh–$T2$ and Rh–Rh). A similar distance (2.68 Å) was found in the octahedral Rh_6 cluster present in the phase Ti_2Rh_6B [9]. The Rh–Rh/$T2$ contacts (see Table 4) are on the average approximately 0.10 Å larger than the distance in metallic rhodium for CN 12 (2.69 Å) [10], but still short enough to be considered as bonding interactions. Even wider contacts have been found in other transition metal rhodium borides, for example in $A_2MRh_5B_2$ with a Rh–Rh range from 2.90 to 3.00 Å (A = Mg, Sc and M = main group and 3d elements) [11] and in $Zn_{10}MRh_{18}B_8$ (average 2.89 Å, with M = 3d elements) [12].

Magnetic properties

The magnetic properties of the compounds $Cr_{0.78(3)}Rh_{6.22(3)}B_3$ and $NiRh_6B_3$ were recorded on a SQUID magnetometer in the temperature range 2 – 400 K at an applied magnetic field B_0 = 1 T. The presentation of the magnetic data follows the recommendation of Hatscher *et al.* (SI units) [13] (Fig. 5). For the $Cr_{0.78(3)}Rh_{6.22(3)}B_3$ phase the recorded molar susceptibility (χ_m) as a function of temperature shows an almost temperature-independent behavior (Pauli paramagnetism, $\chi_m = 6.6 \times 10^{-9}$ m^3 mol^{-1}). For the $NiRh_6B_3$ phase a temperature-dependent behavior is observed at lower temperatures, and the highest measured χ_m value is more than twice that of the temperature-independent value ($\chi_m = 1.8 \times 10^{-8}$ m^3 mol^{-1}) found at higher temperatures. The temperature-independent molar susceptibility in-

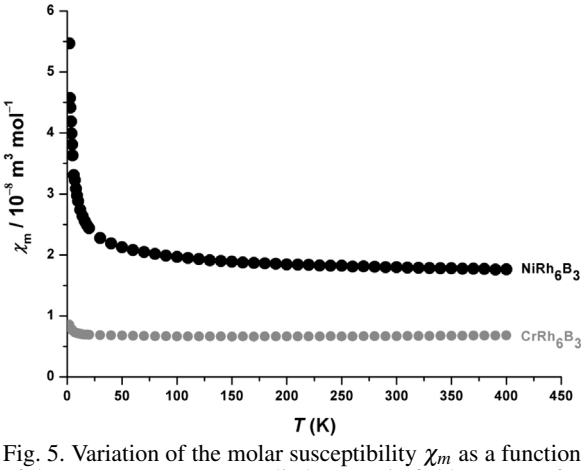

Fig. 5. Variation of the molar susceptibility χ_m as a function of the temperature at an applied magnetic field B_0 = 1 T for $NiRh_6B_3$ (black) and $CrRh_6B_3$ (gray).

creases from $Cr_{0.78(3)}Rh_{6.22(3)}B_3$ to $NiRh_6B_3$, a behavior expected because the number of valence electrons also increases. A similar behavior was also noticed in the $M_{0.5}Ru_{6.5}B_3$ series (M = Cr, Mn, Co, Ni) [4].

No hint of magnetic ordering was observed in $NiRh_6B_3$ down to 2K. This finding is surprising given the fact that the two similar $FeRh_6B_3$ and $CoRh_6B_3$ phases, also containing a ferromagnetic 3*d* metal, were found to order ferromagnetically below relatively high Curie temperatures of 240 and 150 K, respectively. On the other hand, the experimental results for $FeRh_6B_3$ and $CoRh_6B_3$ were confirmed and even extended by first-principles density functional theory calculations which revealed that the magnetic ordering occurs through indirect magnetic coupling between iron (or cobalt) atoms *via* the rhodium atoms [2]. The significant decrease of the magnetic characteristics from the Fe to the Co case correlates with the magnetic moments of the 3*d* elements which decrease from 2.216 μ_B (α-Fe) to 1.715 μ_B (β-Co) [14]. By following this trend the small magnetic moment observed in elemental nickel (0.616 μ_B [14]) is probably not large enough to induce long range magnetic ordering in $NiRh_6B_3$, through indirect magnetic coupling.

Experimental Section

Synthesis and characterization

The starting materials used for the synthesis of the title phases were the following elements: chromium, manganese or nickel (all powders, 99.99 %, Fluka AG), rhodium (100 % Umicore AG & Co.KG, Hanau) and boron (amorphous 97 %, Fluka AG, or crystalline, 99.99 %, Alfa Aesar). These starting materials were first weighed in the corresponding stoichiometric ratio (total mass of each sample 0.20 g) according to the formula "MRh_6B_3" (M = Cr, Mn, Ni) and pressed into pellets. The pelletized powders were then arc-melted on a water-cooled copper crucible (first electrode) under argon atmosphere, by using a direct current of 40 A and a tungsten tip as the second electrode. To insure homogeneity, the ingots were turned over and melted several times. A weight loss during the melting process was observed only for the M = Mn case (about 5 % loss was noticed). The obtained metallic lustrous reguli were mechanically cracked apart and pulverized for examination using a mortar and a pestle.

For the phase identification and the determination of lattice parameters at r. t., powder X-ray methods were applied using a powder diffractometer (Stoe Stadi P, transmission geometry; Cu$K_{\alpha 1}$ radiation (λ = 1.54059 Å), Ge monochromator, image plate detector, and silicon as an internal standard). For EDX measurements with a high resolution, low energy SEM of the type LEO 1530 (Oberkochen, Germany) equipped with an EDX system of the type INCA (Oxford, England) was also used to characterize all metals and their ratios.

Crystal structure determination

Single crystals of suitable sizes were isolated from the powdered samples under an optical microscope for the starting compositions "$CrRh_6B_3$" and "$MnRh_6B_3$". The single-crystal data were collected using a CCD single-crystal diffractometer (Bruker SMART APEX) with graphite-monochromatized MoK_α radiation (λ = 0.71073 Å). The X-ray intensities were corrected for absorption using a semi-empirical procedure [15]. The crystal structures were refined by full-matrix least-squares refinement [16], based on F^2, using anisotropic displacement parameters for all metals and isotropic ones for boron.

Rietveld refinements were also carried out for "MRh_6B_3" (M = Cr, Mn, Ni) powder data by full-matrix least-squares refinement implemented in the program FULLPROF [17]. The starting model for the Rietveld refinements was the single-crystal data of the $FeRh_6B_3$ [3] phase.

Further details of the crystal structure investigation may be obtained from Fachinformationszentrum Karlsruhe, 76344 Eggenstein-Leopoldshafen, Germany (fax: +49-7247-808-666; e-mail: crysdata@fiz-karlsruhe.de, http://www.fiz-informationsdienste.de/en/DB/icsd/depot_anforderung.html) on quoting the deposition number CSD-423675 for $Cr_{0.78(3)}Rh_{6.22(3)}B_3$ and CSD-423676 for $Mn_{0.39(3)}Rh_{6.61(3)}B_3$.

Magnetic measurements

Temperature-dependent susceptibility data for polycrystalline "MRh_6B_3" (M = Cr, Ni) samples were performed

with a SQUID magnetometer (MPMS-5S, Quantum Design) in the temperature range 2 – 400 K at applied fields B_0 = 0.01 – 1 T. The data were corrected for the sample holder (Teflon® tubes).

Conclusion

The ternary boride phases $M_xRh_{7-x}B_3$ (M = Cr, Mn, Ni; x = 0.39 – 1) have been synthesized and characterized by powder and single-crystal X-ray diffraction as well as EDX analysis. They crystallize in the Th_7Fe_3 structure type. In all crystal structures, the M atom is found (mixed with rhodium) preferentially at one of the three available rhodium sites. Magnetic properties investigations have shown a temperature-independent (Pauli) paramagnetism for the Cr-based phase, whereas for the Ni-based phase an additional strong temperature dependence was observed below 250 K.

Acknowledgements

The authors wish to acknowledge Deutsche Forschungsgemeinschaft for financial support (DFG fellowship to Priv.-Doz. Dr. B. P. T. Fokwa), K. Kruse for technical support during the X-ray experiments and R. Zaunbrecher (IPC, RWTH Aachen) for the EDX analyses.

[1] B. P. T. Fokwa, R. Dronskowski, *J. Alloys Compd.* **2007**, *428*, 84 – 89.
[2] P. R. N. Misse, M. Gilleßen, B. P. T. Fokwa, *Inorg. Chem.* **2011**, *50*, 10303 – 10308.
[3] B. P. T. Fokwa, R. Dronskowski, *Z. Anorg. Allg. Chem.* **2005**, *631*, 2478 – 2780.
[4] P. R. N. Misse, B. P. T. Fokwa, *Z. Anorg. Allg. Chem.* **2010**, *636*, 1013 – 1017.
[5] B. Aronsson, E. Stenberg, J. Aselius, *Acta Chem. Scand.* **1960**, *14*, 734 – 741.
[6] P. Villars, K. Cenzual, *Pearson's Crystal Structure Database for Inorganic Compounds* (on CD-ROM), (version 1.0), Materials Park, OH, (USA), **2007/8**.
[7] J. A. Dean, *Lange's Handbook of Chemistry*, 15th ed., McGraw-Hill, New York, **1999**.
[8] T. Shishido, J. H. Ye, S. Okada, K. Kudou, T. Sasaki, S. Isida, T. Naka, M. Oku, I. Higashi, H. Kishi, H. Horiuchi, T. Fukuda, *J. Alloys Compd.* **2000**, *309*, 107 – 112.
[9] B. P. T. Fokwa, B. Eck, R. Dronskowski, *Z. Kristallogr.* **2006**, *221*, 445 – 449.
[10] L. Pauling, B. Kamb, *Proc. Natl. Acad. Sci. USA* **1986**, *83*, 3569 – 3571.
[11] E. A. Nagelschmitz, W. Jung, R. Feiten, P. Müller, H. Lueken, *Z. Anorg. Allg. Chem.* **2001**, *627*, 523 – 532
[12] U. Eibenstein, W. Jung, *Z. Anorg. Allg. Chem.* **1998**, *624*, 802 – 806
[13] S. T. Hatscher, H. Schilder, H. Lueken, W. Urland, *Pure Appl. Chem.* **2005**, *77*, 497 – 511.
[14] H. Lueken, *Magnetochemie*, Teubner, Stuttgart, Leipzig, **1999**.
[15] G. M. Sheldrick, SADABS, Program for Empirical Absorption Correction of Area Detector Data, University of Göttingen, Göttingen (Germany) **2001**.
[16] G. M. Sheldrick, *Acta Crystallogr.* **2008**, *A64*, 112 – 122.
[17] J. Rodríguez-Carvajal, FULLPROF, A Program for Rietveld Refinement and Pattern Matching Analysis, Institut Laue-Langevin, Grenoble (France) **2004**.